

# Investigation and analysis of interleaved dc-dc boost converter for grid-connected photovoltaic energy system

Mehmet Büyük

Adıyaman University, Electrical and Electronics Engineering, 02300, Adıyaman, Türkiye, [mbuyuk@adiyaman.edu.tr](mailto:mbuyuk@adiyaman.edu.tr),  
ORCID: 0000-0003-3026-4034

## ABSTRACT

The installation of photovoltaic energy system has been increasing in recent years with the increment of the demand to the electrical power. PV system can be installed as either standalone or grid-connected. Grid-connected PV systems are more attractive because of not requiring a storage system. In this study, a three-leg interleaved boost converter for grid-connected PV system is proposed. In the proposed system, a grid-connected PV system is designed and modelled in a simulation environment. The proposed model is analysed in comparison with the conventional dc-dc boost converter topology under variations of irradiance and temperature. The comparison of two systems is performed according to input current ripple ratio and THD value of the grid current. The simulation results show that the proposed topology has lower current ripple and THD value comparing with the conventional topology.

## ARTICLE INFO

### Research article

Received: 26.10.2022

Accepted: 16.12.2022

### Keywords:

*dc/dc converter, interleaved boost converter, grid-connected PV system, current ripple, THD.*

## 1. Introduction

In today's life, the applications of renewable energy sources have come into prominence by reduction of the fossil fuels and increasing greenhouse gas emissions [1, 2]. Photovoltaic (PV) panel systems attract further attention since their simple implementation and low maintenance cost. In addition, the power generation capacity of PV systems can be improved via implementation of industry 4.0 [3]. Besides, the systems are applicable for houses, industrial plants and commercial power plants [4-7]. Furthermore, the installed PV system capacity over the world has been increasing significantly in recent years [8]. Although standalone and grid-connected PV panel systems are available in applications, the grid-connected systems are more efficient and highly preferred systems in applications [5-7]. In general, a dc/dc converter and an inverter are used to connect the PV panels to the grid [9]. The dc/dc converter is applied to obtain the suitable dc voltage level with the maximum power of PV panel [1, 10, 11]. The inverter is utilised to converter dc voltage into ac voltage [12].

There are several dc/dc converter topologies implemented in the grid-connected PV systems. However, a boost converter is usually preferred as a dc/dc converter in PV system and renewable energy systems [2, 13-16]. There are also a few boost converter circuits in literature studies and applications [13, 17, 18]. In earlier studies, conventional boost converter topology is used with PV system. However, the PV current

has a high ripple ratio when the conventional boost converter is used [10, 11, 19, 20]. The high current ripple ratio in PV side effects total harmonic distortion (THD) value of current injected to the grid. Besides, the high ripple degrades the PV lifetime and overall system efficiency.

In this study, a three-leg interleaved boost converter is applied for the grid-connected PV system. The proposed system is modelled and analysed through a simulation environment. A grid-connected PV system in the rating of 10.6 kW is designed and constructed in the simulation environment, and the constructed model is simulated for conventional boost converter and IBC systems. The modelled system is examined under different irradiance and temperature values. The simulation results are presented by considering current ripple ratio and THD value.

The rest of the manuscript is organized as follows. In Section 2, the PV system model of the simulated system and its characteristics are introduced. In Section 3, the structure of the proposed system is presented. By this way, the model of the proposed system is explained in detail. In addition, the current ripple ratios are given for the conventional boost converter and IBC. In Section 4, the simulation results of the proposed system with the conventional boost converter and IBC topologies are presented. The results of IBC topology are discussed and compared with the results of the conventional topology. The conclusion is discussed in Section 5.

## 2. PV system model and characteristic

A PV module consists of small solar cells (approximately 1-2 W) to generate high output power and voltage. As well known that an ideal solar cell is modelled as a current source with parallel a diode. Besides, series and parallel resistors are included to ideal model to demonstrate power losses. The widespread equivalent circuit model of a single PV cell/module is illustrated in Figure 1. This model is called a single diode model and includes five parameters to be determined. The  $I - V$  characteristic of the single diode model is acquired through Eq. (1) [21].

$$I = I_{pv} - I_0 \left[ \exp \left( \frac{V + IR_s}{aV_T} \right) - 1 \right] - \frac{V + IR_s}{R_{sh}} \quad (1)$$

Where,

- $I_{pv}$  : PV current
- $I_0$  : Saturation current
- $R_s$  : Series resistor
- $R_{sh}$  : Shunt resistor
- $V_T$  : Diode thermal voltage

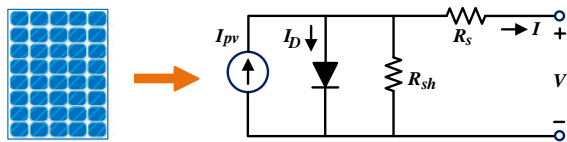


Figure 1. A single PV module and its equivalent circuit scheme

The parameters of the model are obtained by equations of short circuit, open circuit, MPP circuit and zero derivative for MPP circuit. The parameters for a single module are shown in Table 1. According to these parameters, PV current, series and shunt resistors and diode saturation current are obtained. Then, the  $I - V$  and  $P - V$  curves of this model are drawn for different irradiance values at 25 °C, as shown in Figure 2.

Table 1. The parameters for a single PV module

Parameter	Description	Value
$P_{mp}$	Maximum power	305.2 W
$V_{oc}$	Open circuit voltage	64.14 V
$V_{mp}$	Voltage at MPP	54.7 V
$N_{cell}$	# of cell per module	96
$I_{sc}$	Short-circuit current	5.94 A
$I_{mp}$	Current at MPP	5.56 A

The voltage level of the single module is low during the grid connection. Thus, in the present work, seven in series and five in parallel modules are connected to create a PV array with sufficient voltage level and high current value. The  $I - V$  and  $P - V$  curves of PV array are drawn for different irradiance values at 25 °C, as demonstrated in Figure 3.

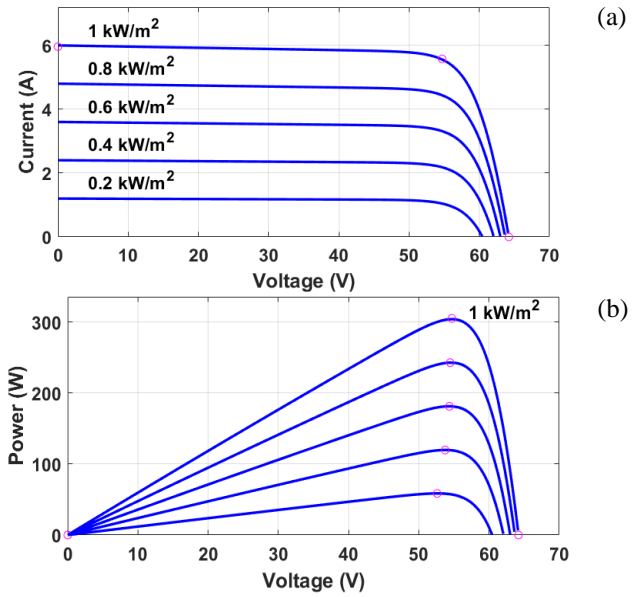


Figure 2. The  $I - V$  and  $P - V$  curves of single PV module under different irradiances

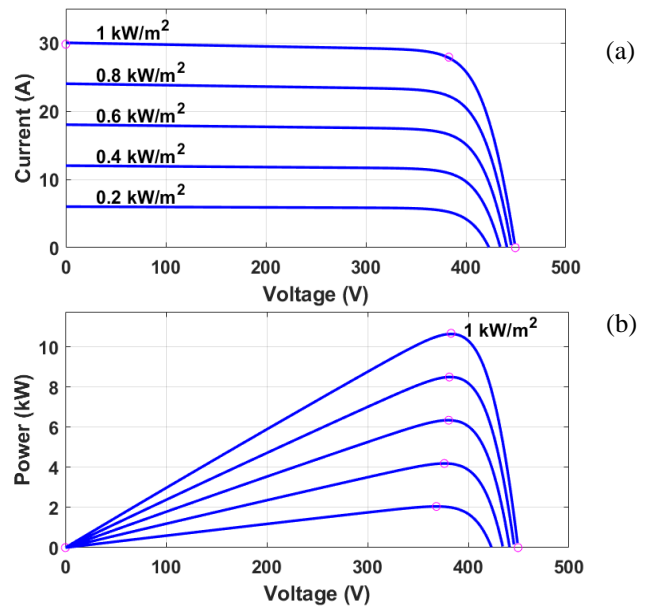
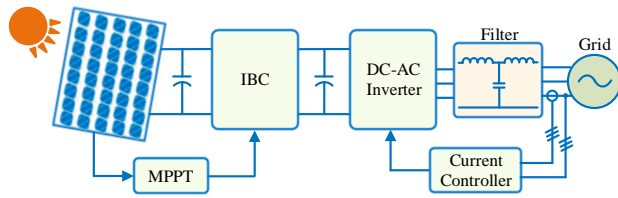


Figure 3. The  $I - V$  and  $P - V$  curves of PV array under different irradiances

## 3. Structure and control of the proposed system model

The general representation of the proposed system is demonstrated in Fig. 4. The proposed system consists of a PV array transferring solar energy into electric energy, a three-leg boost converter with MPPT controller, and a three-phase DC-AC inverter with the current controller and output LCL filter. Incremental conductance MPPT algorithm is applied to acquire maximum power [22,23].



**Figure 4.** General structure scheme of the proposed system

3.1. Interleaved boost converter

The conventional boost converter and IBC structures with pulses and PV currents are shown in Figure 5. The structure and pulse signal of the conventional converter are demonstrated in Figure 5(a) and Figure 5(c). Besides, the

structure and pulse signals of IBC topology are shown in Figure 5(b) and Figure 5(d).

The relation between input voltage and output voltage of the conventional boost converter is given in (2). The current flowing on the inductor is increasing once the switching component turns on and decreasing when turns off. The difference between the lower and upper points of the current is ripple current that has drawbacks on the PV system and output voltage. The ripple current is obtained by Eq. (3). To lessen the ripple current, the inductance value or switching frequency can be increased. However, higher inductance value results in bulky system and high switching frequency leads to efficiency degradation. In this study, instead, a three-leg boost converter is proposed to reduce the inductor current ripple and its negative effect [13, 24].

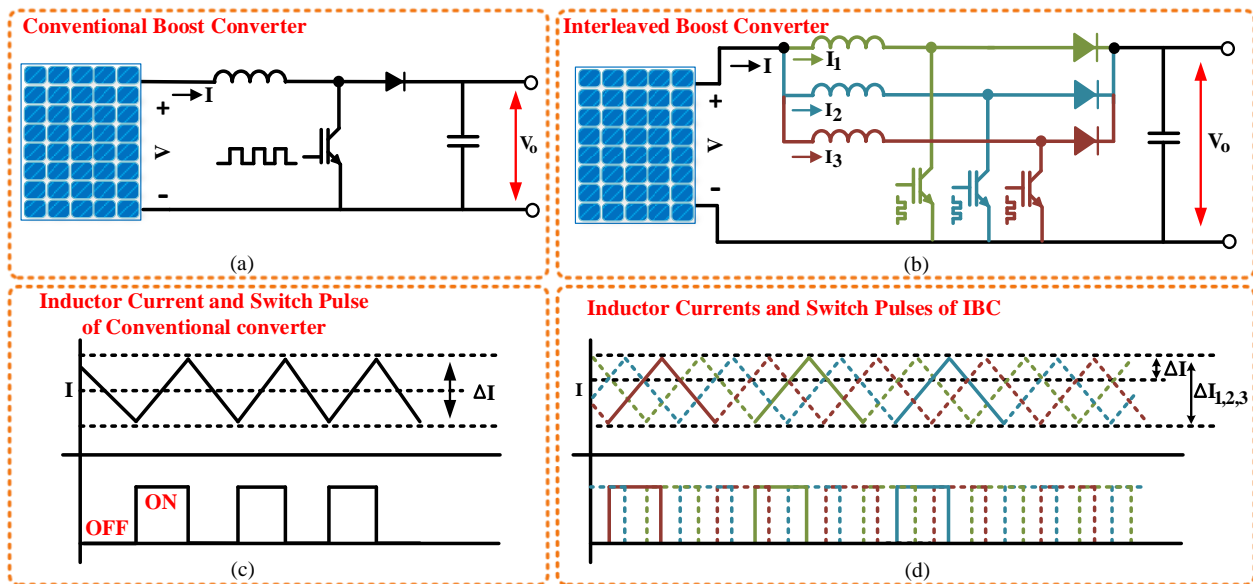


**Figure 5.** The structures, currents and pulse waveforms of the conventional boost converter and IBC

$$V_o = \frac{1}{(1 - D)} V \tag{2}$$

$$\Delta I = \frac{DT_s}{L} V \tag{3}$$

Where,  $D$  is duty cycle and  $T_s$  is switching time.

In this study, a three-phase IBC is preferred to convert DC voltage level. Three parallel converters are used in this topology, as shown in Figure 5(b). The operation of IBC is based on applying identical pulses with shifting the pulses of the switches by  $120^\circ$  [19,24]. The switching signals and inductor currents are demonstrated in Figure 5(d). The switching signals may overlap depending on duty cycle, as shown in Figure 5(d). It is proposed to select the duty cycle higher than  $1/3$  in order to obtain boosted input voltage. The

input ripple current is obtained as Eq. (4). The input ripple current is obtained according to the duty cycle ratio [10].

$$\Delta I = \begin{cases} 0.34 < D < 0.66 & ; \frac{VT_s d}{3L} \left( \frac{2 - 3D}{D'} \right) \\ 0.67 < D < 1 & ; \frac{VT_s d}{L} \left( \frac{1 - D}{D'} \right) \end{cases} \tag{4}$$

Where,  $d$  is the ratio of input current rising time to its period ( $t_r/\tau$ ).

3.1. DC/AC conversion

The PV system is connected to the grid through a DC-AC inverter. In this study, a three-phase inverter is used to convert DC voltage into AC voltage. The inverter includes three half-bridge inverter legs. The switching components of the inverter are modulated by SPWM method. The rms voltage value of

inverter is obtained as in (5) for the fundamental component [25]. The circuit diagram of the grid-connected inverter is demonstrated in Figure 6. An LCL filter is tied between the inverter and the grid to effectively degrade the ripple harmonics generated from the modulation of the inverter [26]. Besides, a simple resistor connected in series with the filter capacitor suppresses the filter resonance.

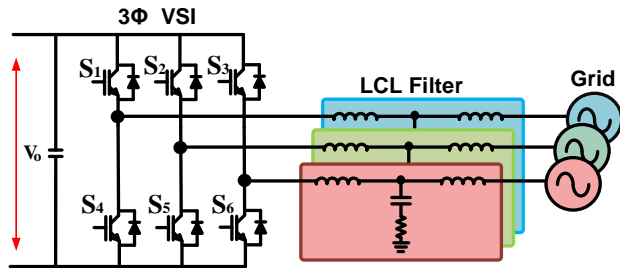


**Figure 6.** The circuit diagram of the three-phase grid-connected inverter

$$V_i = \frac{M}{2\sqrt{2}} V_o \tag{5}$$

Where, M index represents the modulation ratio of the reference sine signal to the carrier signal.  $V_i$  and  $V_o$  are inverter output fundamental voltage and capacitor dc voltage, respectively. The constant  $M/(2\sqrt{2})$  gives the inverter gain value [25].

**4. Case studies and discussion**

The proposed system is modelled and analysed through a simulation program environment. The system parameters of the modelled system are given in Table 2. The proposed system is tested under various irradiance and temperature values. The changes in irradiance and temperature are shown in Figure 7. Besides, the mean powers obtained from PV array according to the irradiance and temperature variations for conventional boost converter and IBC are illustrated in Figure 8. The mean power obtained by the IBC topology is always higher than the conventional topology.

The modelled system is examined for conventional boost converter and three-phase IBC topologies. Figure 9 shows the current and voltage waveforms once the conventional boost converter and three-phase IBC are applied. It is obvious that the output current has high ripple current when the conventional method is used. On the other hand, the ripple current is reduced to almost 1/3 ratio with IBC technique.

**Table 2.** The system parameters of the proposed system

Parameter	Description	Value
$V_g$	Grid voltage	380 V
$f_g$	Grid frequency	50 Hz
$V_o$	DC link voltage	750 V
$P_{pv}$	Max. PV power	10.6 kW
$f_{sd}$	IBC switching freq.	5 kHz
$f_{si}$	Inverter switching freq.	5 kHz

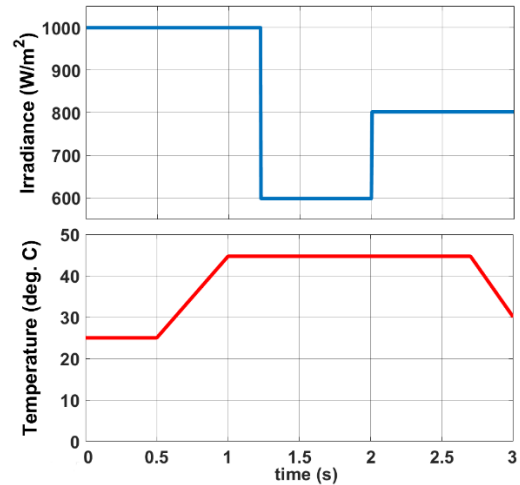


**Figure 7.** The changes in irradiance and temperature

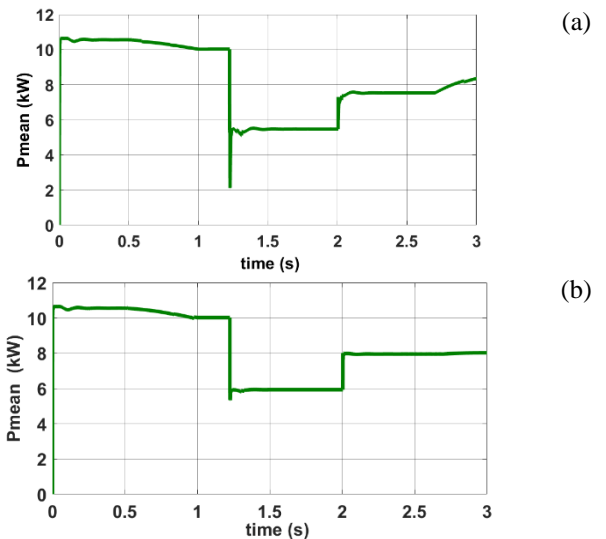


**Figure 8.** Mean power behaviour of PV array under irradiance and temperature changes for conventional converter and (b) IBC topology

The grid voltage and current supplied by PV to the grid under the variation of the irradiance and temperature are shown in Figure 10. This result is illustrated only for IBC based topology. It can be seen from the figure that the supplied current decreases with irradiance reduction and temperature increment.

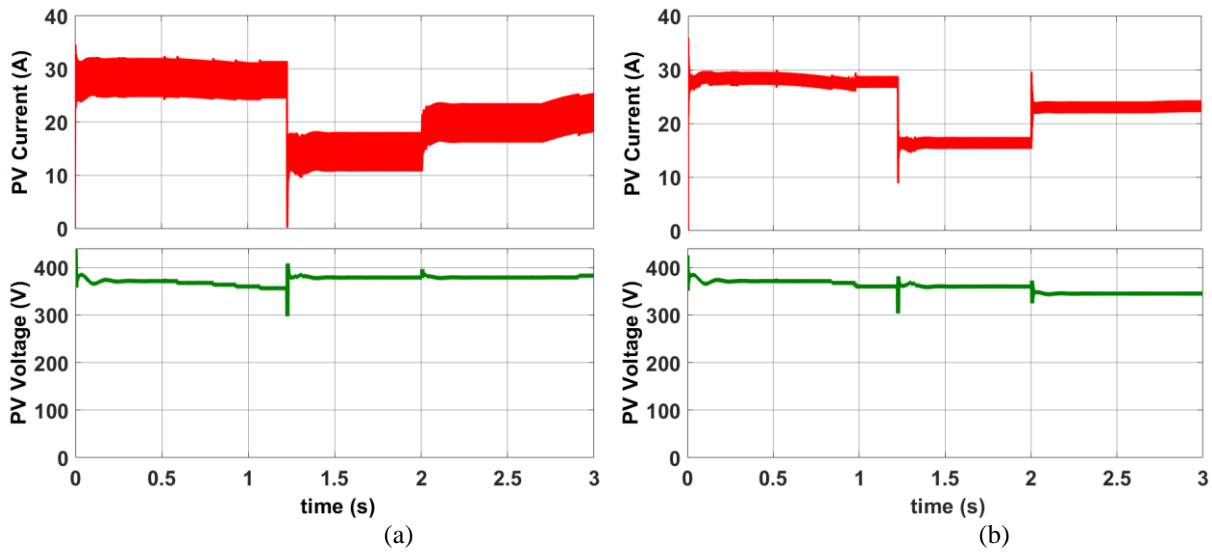


Figure 9. Output current and voltage waveforms of PV array for (a) conventional boost converter and (b) IBC

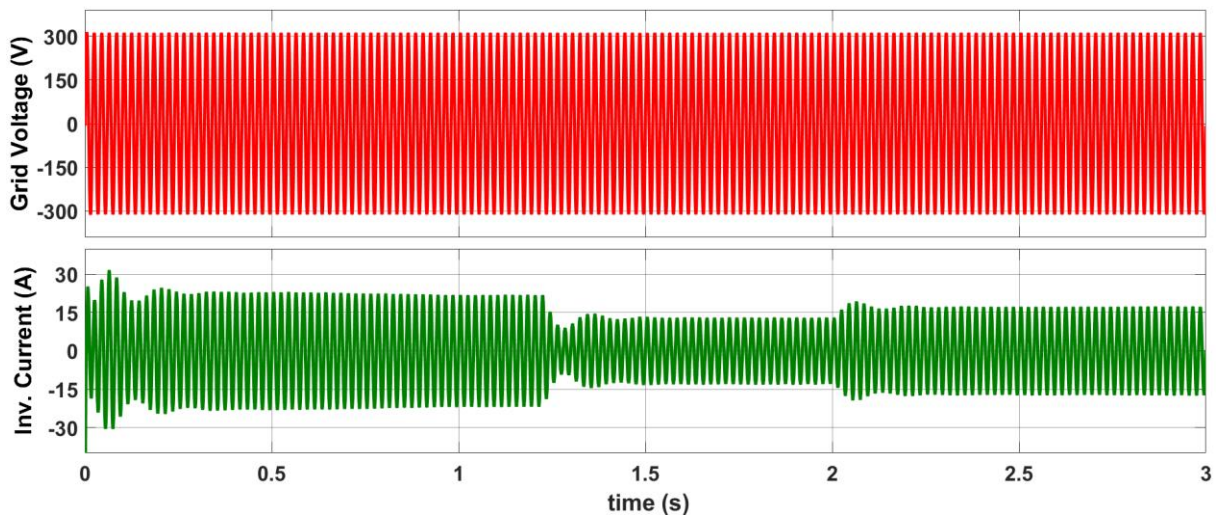
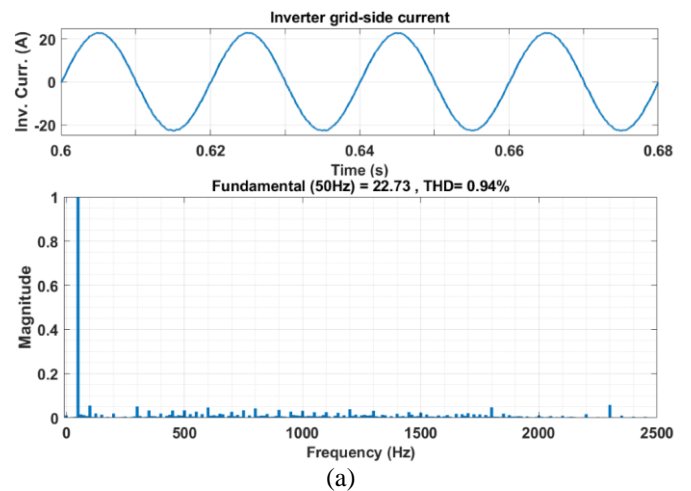
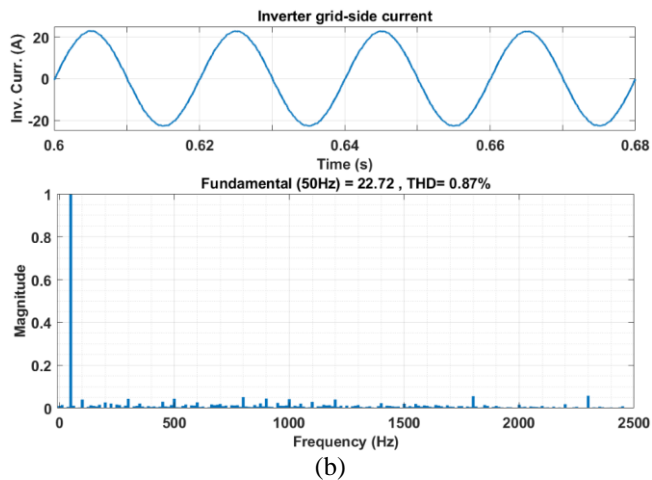


Figure 10. The waveforms of grid voltage and inverter current

The grid-side current waveforms with their harmonic spectra and THDs are shown in Figure 11. The results for conventional and IBC methods are given in Figure 11(a) and Figure 11(b), respectively. The THD values of the grid-side currents are 0.94 % and 0.87 % for the conventional method and IBC method, respectively. It is obvious from the simulation results that the proposed system injects current to the grid with lower THD value.







**Figure 11.** Waveforms of grid currents and FFTs with (a) conventional method and (b) IBC structure

## 5. Conclusion

A grid-connected PV system with IBC has been proposed in this study. In the proposed study, IBC is used as dc/dc converter to reduce the current ripple ratio. The IC MPPT algorithm is applied to obtain the maximum power from the PV array. A 10.6 kW grid-connected PV system is designed in this study. The proposed system has been modelled in simulation environment, and it is examined under variation of irradiance and temperature. The proposed system is compared with the conventional boost converter model. It is shown from the simulation results that the IBC topology has a lower PV current ripple in comparison with the conventional boost converter. The current ripple values are 7.2V and 2.1V for the conventional boost converter and the IBC topologies, respectively. Moreover, the THD values of the grid current are 0.94% and 0.87% for the conventional boost converter and the IBC topologies, respectively. It is obvious from the results that the current ripple and THD value are reduced by the IBC model.

## References

- [1]. M. İnci, "Interline fuel cell (I-FC) system with dual-functional control capability," *International Journal of Hydrogen Energy*, vol. 45, pp. 891-903, 2020/01/01/ 2020.
- [2]. Sudha R., Abishri P., and U. S., "Review of Coupled Two and Three Phase Interleaved Boost Converter (IBC) and Investigation of Four Phase IBC for Renewable Application," *International Journal of Renewable Energy Research*, vol. 6, 2016.
- [3]. H. H. Çoban, "Accelerating renewable energy generation over industry 4.0 " *MANAS Journal of Engineering*, vol. 7, pp. 114-120, 2019.
- [4]. X. Cao, C. Zhang, Y. Zhang, Z. Gan, H. Li, W. Ni, et al., "The simulation study of the modulation method for PV grid-connected system," *Energy Procedia*, vol. 145, pp. 122-127, 2018/07/01/ 2018.
- [5]. M. İnci, "Design and Analysis of Dual Level Boost Converter Based Transformerless Grid Connected PV System for Residential Applications," in *2019 4th International Conference on Power Electronics and their Applications (ICPEA)*, 2019, pp. 1-6.
- [6]. F. Sedaghati, A. Nahavandi, M. A. Badamchizadeh, S. Ghaemi, and M. Abedinpour Fallah, "PV Maximum Power-Point Tracking by Using Artificial Neural Network," *Mathematical Problems in Engineering*, vol. 2012, p. 506709, 2012/03/01 2012.
- [7]. S. Zhang and Y. Tang, "Optimal schedule of grid-connected residential PV generation systems with battery storages under time-of-use and step tariffs," *Journal of Energy Storage*, vol. 23, pp. 175-182, 2019/06/01/ 2019.
- [8]. M. K. A. Rödl , H. Schaumburg, "Strategy For A Large Scale Introduction Of Solar Energy In Central Asia," *MANAS Journal of Engineering* vol. 5, pp. 48-56, 2017.
- [9]. M. S. Aygen and M. İnci, "Zero-sequence current injection based power flow control strategy for grid inverter interfaced renewable energy systems," *Energy Sources, Part A: Recovery, Utilization, and Environmental Effects*, pp. 1-22, 2020.
- [10]. G.-Y. Choe, J. Kim, H.-S. Kang, and B.-K. Lee, "An Optimal Design Methodology of an Interleaved Boost Converter for Fuel Cell Applications," *Journal of Electrical Engineering & Technology* vol. 5, pp. 319-328, 2010.
- [11]. M. Elsieid, A. Oukaour, H. Chaoui, H. Gualous, R. Hassan, and A. Amin, "Real-time implementation of four-phase interleaved DC–DC boost converter for electric vehicle power system," *Electric Power Systems Research*, vol. 141, pp. 210-220, 2016/12/01/ 2016.
- [12]. M. İnci, "Performance Analysis of T-type Inverter Based on Improved Hysteresis Current Controller," *Balkan Journal of Electrical and Computer Engineering*, vol. 7, pp. 149-155, 2019.

- [13]. J. Seok and A. Parastar, "Modeling and Control of the Average Input Current for Three-Phase Interleaved Boost Converters," *IEEE Transactions on Industry Applications*, vol. 51, pp. 2340-2351, 2015.
- [14]. R. Seyezhai and B. L. Mathur, "Design and implementation of interleaved boost converter for fuel cell systems," *International Journal of Hydrogen Energy*, vol. 37, pp. 3897-3903, 2012/02/01/ 2012.
- [15]. F. Slah, A. Mansour, M. Hajer, and B. Faouzi, "Analysis, modeling and implementation of an interleaved boost DC-DC converter for fuel cell used in electric vehicle," *International Journal of Hydrogen Energy*, vol. 42, pp. 28852-28864, 2017/11/30/ 2017.
- [16]. P. Thounthong, P. Sethakul, S. Rael, and B. Davat, "Design and Implementation of 2-Phase Interleaved Boost Converter for Fuel Cell Power Source," in 2008 4th IET Conference on Power Electronics, Machines and Drives, 2008, pp. 91-95.
- [17]. R. Saadi, M. Y. Hammoudi, O. Kraa, M. Y. Ayad, and M. Bahri, "A robust control of a 4-leg floating interleaved boost converter for fuel cell electric vehicle application," *Mathematics and Computers in Simulation*, vol. 167, pp. 32-47, 2020/01/01/ 2020.
- [18]. J. Choi, H. Cha, and B. Han, "A Three-Phase Interleaved DC-DC Converter With Active Clamp for Fuel Cells," *IEEE Transactions on Power Electronics*, vol. 25, pp. 2115-2123, 2010.
- [19]. D. S. G. Krishna and M. Patra, "Modeling of multi-phase DC-DC converter with a compensator for better voltage regulation in DC micro-grid application," in 2016 International Conference on Signal Processing, Communication, Power and Embedded System (SCOPEs), 2016, pp. 989-994.
- [20]. M. Rezvanyvardom, E. Adib, and H. Farzanehfard, "New interleaved zero-current switching pulse-width modulation boost converter with one auxiliary switch," *IET Power Electronics*, vol. 4, pp. 979-983, 2011.
- [21]. J. Cubas, S. Pindado, and C. De Manuel, "Explicit Expressions for Solar Panel Equivalent Circuit Parameters Based on Analytical Formulation and the Lambert W-Function," *Energies*, vol. 7, pp. 4098-4115, 2014.
- [22]. S. Motahhir, A. El Hammoumi, and A. El Ghzizal, "The most used MPPT algorithms: Review and the suitable low-cost embedded board for each algorithm," *Journal of Cleaner Production*, vol. 246, p. 118983, 2020/02/10/ 2020.
- [23]. A. Loukriz, M. Haddadi, and S. Messalti, "Simulation and experimental design of a new advanced variable step size Incremental Conductance MPPT algorithm for PV systems," *ISA Transactions*, vol. 62, pp. 30-38, 2016/05/01/ 2016.
- [24]. S. Sakulchotruangdet and S. Khwan-on, "Three-phase Interleaved Boost Converter with Fault Tolerant Control Strategy for Renewable Energy System Applications," *Procedia Computer Science*, vol. 86, pp. 353-356, 2016/01/01/ 2016.
- [25]. M. Nabil, S. M. Allam, and E. M. Rashad, "Modeling and design considerations of a photovoltaic energy source feeding a synchronous reluctance motor suitable for pumping systems," *Ain Shams Engineering Journal*, vol. 3, pp. 375-382, 2012/12/01/ 2012.
- [26]. M. Büyük, A. Tan, M. Tümay, and K. Ç. Bayındır, "Topologies, generalized designs, passive and active damping methods of switching ripple filters for voltage source inverter: A comprehensive review," *Renewable and Sustainable Energy Reviews*, vol. 62, pp. 46-69, 2016/09/01/ 2016..